

## UC Davis

### UC Davis Previously Published Works

**Title**

Calculated Oxygen-Isotope Fractionations among Brucite, Portlandite, and Water

**Permalink**

<https://escholarship.org/uc/item/6mh2h41z>

**Journal**

ACS Earth and Space Chemistry, 3(8)

**ISSN**

2472-3452

**Authors**

Colla, Christopher A  
Casey, William H

**Publication Date**

2019-08-15

**DOI**

10.1021/acsearthspacechem.9b00020

Peer reviewed

# Calculated Oxygen-Isotope Fractionations among Brucite, Portlandite, and Water

Christopher A. Colla<sup>\*,†</sup> and William H. Casey<sup>‡,§</sup>

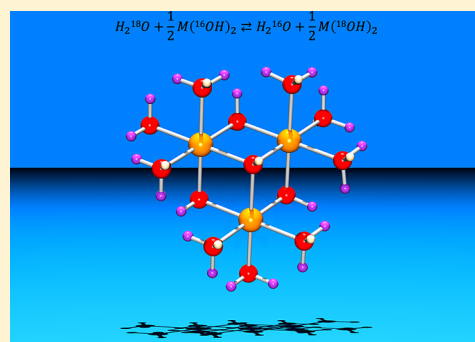
<sup>†</sup>Geochemistry Department, Energy Geosciences Division, Lawrence Berkeley National Laboratory, 1 Cyclotron Road, Berkeley, California 94720, United States

<sup>‡</sup>Department of Chemistry and <sup>§</sup>Department of Earth and Planetary Sciences, University of California, 1 Shields Avenue, Davis, California 95616, United States

## Supporting Information

**ABSTRACT:** The oxygen-isotope fractionations between brucite and water, portlandite and water, and brucite and portlandite have been calculated over the temperature range of 0 to 450 °C using quantum-chemical methods and several basis sets and functionals. The calculations also employ embedded clusters that are chosen using the Pauling-bond-strength-conserving termination method that maintains a neutral cluster with fractional charges assigned to terminal atoms. These calculations improve upon the previous semiempirical methods for predicting mineral–mineral fractionations. These semiempirical methods fail to accurately predict the relative enrichment and depletion of oxygen isotopes for the brucite–portlandite pair. The quantum calculations presented here also fail to predict at the absolute values for enrichment of oxygen isotopes between minerals and water, and a simple correction must be employed to achieve agreement with experiments if water is in the reaction. No such correction is needed to predict fractionation between minerals. The trends derived from the calculations are robust to changes in basis sets and functionals.

**KEYWORDS:** *Oxygen isotopes, Electronic structure, Brucite, Portlandite, Isotope fractionation, Density functional theory*



## INTRODUCTION

Among the most useful geochemical tools for understanding mass movements in the Earth are the stable isotopes that fractionate between phases and among molecules. Oxygen isotopes are particularly useful, because most rock-forming minerals are oxides, and many reactions involve oxygen molecules in the atmosphere or water in the hydrosphere. The fractionation of oxygen isotopes depends strongly on temperature; hence, the isotopic record can provide geothermometry, as well as providing information about the elemental provenance.

Attempts to calculate isotope fractionations date back to some of the early pioneering work by Urey<sup>1</sup> in 1947 and extend to the present. For a comprehensive review of light-isotope fractionation among gaseous molecules and the quantum- and statistical-mechanical theories behind this fractionation, the reader is directed to, among several notable works, Richet et al.<sup>2</sup> and Chacko et al.<sup>3</sup> Notably, the fractionation of hydrogen and oxygen isotopes between water and low-temperature metal-hydroxide minerals, in particular kaolinite, has been calculated using first-principles plane-wave DFT methods.<sup>4</sup> Using the same plane-wave calculations of Méheut et al.,<sup>4</sup> the same group calculated the D/H fractionation among hydrous minerals brucite, kaolinite, lizardite, and gibbsite and water.<sup>5</sup> Prior to the efforts of Méheut et al.,<sup>4,5</sup> Reynard and Caracas<sup>6</sup> carried out similar

calculations of D/H fractionation between brucite and water, using similar plane-wave methods and pointing out the benefit of using brucite  $[Mg(OH)_2(s)]$  in theoretical studies, because so much experimental work is available for this mineral. Blanchard et al.<sup>7</sup> calculated reduced-partition-function ratios (RPF) of iron and oxygen in goethite, finding a discrepancy between their results and the previous semiempirical predictions. Of particular note is a recent paper by Asaduzzaman and Ganguly,<sup>8</sup> who treated D/H isotopic exchange for epidote and water via quantum calculations. Their equations closely resemble those used here, because the ratio of exchanging sites is 2:1 in their study and is 1:2 here.

Unlike nontraditional medium-mass elements, such as Mg and Ca, which exhibit smaller stable-isotope fractionations between minerals and aqueous ions, on the order of 1–2 per mil, oxygen-isotope fractionations can range from 5 to 10 per mil. These larger fractionations makes oxygen isotopes better for simulation, because statistically significant fractionations can be achieved efficiently, that is, without averaging over many molecular conformations.

Received: January 19, 2019

Revised: May 13, 2019

Accepted: May 17, 2019

Published: May 22, 2019

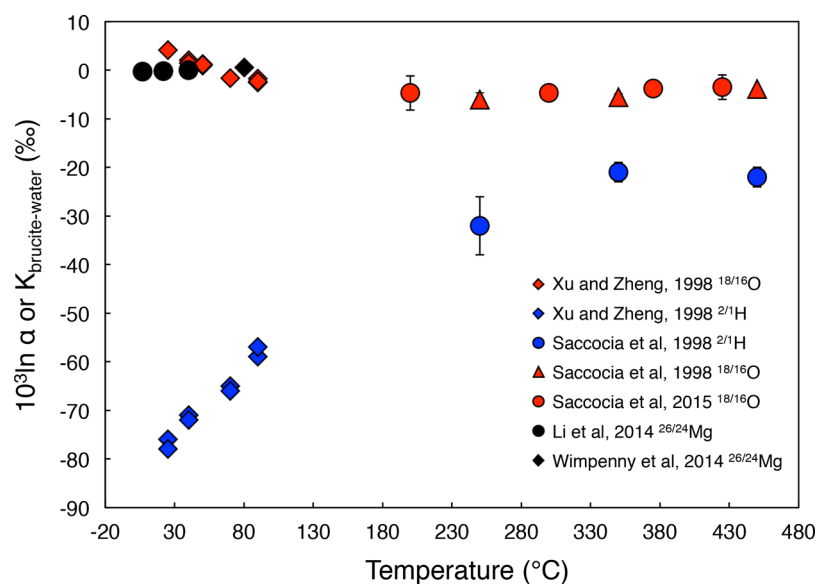


**Figure 1.** Experimental fractionation factors,  $10^3 \ln(\alpha)$ , between brucite and water as a function of temperature. Note that oxygen- and hydrogen-isotope fractionation factors approach one another with increased temperature.

A long-standing method of predicting oxygen-isotope fractionations for mineral–water systems has been the semiempirical, increment method of Zheng.<sup>9–13</sup> The increment method was established as an alternative to expensive computer calculations and is quite accessible. Complete discussion of this model is beyond the scope here, but it is based on a summation of two terms, one that accounts for metal–oxygen bond strengths and a second, unitless function that accounts for isotopic substitution. The bond strengths are estimated from the cation coordination numbers, the cation formal valence, and the ionic radii. Central to the method, however, is a normalization step that employs an experimental  $\langle \text{Si–O} \rangle$  bond distance in quartz as an essential empirical parameter. Semiempirical methods such as the increment method are particularly useful, because they can cheaply predict fractionations at temperatures that are difficult to achieve experimentally.<sup>14</sup> However, first-principles calculations could replace the semiempirical methods if they improve accuracy at little computational cost, since computing power has increased enormously since the semiempirical model was built. Unlike semiempirical methods, first-principles calculations do not rely on empirical data but on solutions to the energy of a many-particle system, which can be solved using density-functional-theory methods (DFT) of varying levels of sophistication.

All isotopic systems for brucite have been studied experimentally, including  $^{26/24}\text{Mg}$ ,  $^{18/16}\text{O}$ , and  $^{2/1}\text{H}$ . Oxygen- and hydrogen-isotope equilibrium have been explored from ambient temperatures to 450 °C, and hydrogen-isotope fractionation between brucite and water has been determined as a function of pressure.<sup>14–18</sup> Horita et al.<sup>17</sup> determined the deuterium/protium fractionation between brucite and pure water from 15 to 800 MPa and at 380 °C. Over this pressure range, Horita and co-workers found that the fractionation factor increased systematically with pressure by 12.4 per mil.<sup>17</sup> Saccocia et al.<sup>15</sup> and Saccocia et al.<sup>14</sup> conducted high-temperature experiments at two pressures, ambient and 50 MPa. It is important to note that oxygen-isotope fractionation in the brucite–water system does not seem to be affected by pressure, unlike hydrogen-isotope fractionation.<sup>17</sup> When all

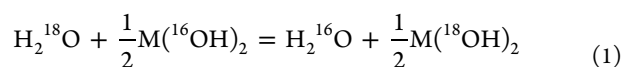
isotopic data are plotted together, the oxygen- and hydrogen-isotope fractionations approach one another and appear to converge at temperatures of  $\sim 450$  °C (see Figure 1). There is a large positive  $^{18}\text{O}/^{16}\text{O}$  fractionation for brucite near room temperature (+4 per mil), but it decreases to  $-2$  per mil at 70 °C.

Previously, experimental work describing  $^{26/24}\text{Mg}$  fractionation in the brucite–aqueous system indicated a temperature-dependent isotope-exchange reaction between aqueous Mg and brucite (see black symbols in Figure 1). At elevated temperatures, ( $\sim 80$  °C), brucite is slightly isotopically heavy with respect to magnesium solutes in the aqueous solution, which are overwhelmingly dominated by the  $[\text{Mg}(\text{OH}_2)_6]^{2+}$ .<sup>19–21</sup> Predictions of  $^{26/24}\text{Mg}$  fractionation indicated that the measured temperature dependence could only be achieved by fixing  $\langle \text{Mg–O} \rangle$  bond distances in the aqueous ion,  $[\text{Mg}(\text{OH}_2)_6]^{2+}$ . The key conclusion was that these bond lengths were much more important than details of outer-sphere solvation in the model cluster. It is also clear that DFT methods overestimate metal–oxygen bond distances for hydrated ions if unconstrained, indicating that the  $[\text{Mg}(\text{OH}_2)_6]^{2+}$  ion probably has shorter  $\langle \text{Mg–O} \rangle$  bond distances than  $\langle \text{Mg–O} \rangle$  in solids.<sup>22</sup>

Here we use DFT, MP2, and the embedded-cluster approach to predict reduced-partition-function ratio (RPF) values for oxygen-isotope fractionations, leading to estimates of the fractionation factors among water and two hydroxide minerals, brucite and portlandite. The minerals brucite and portlandite are ideal for study because of the abundance of experimental data, as mentioned above, but also because they have only one oxygen site in the structure. In the bulk structures, three metal atoms and a hydroxide proton tetrahedrally coordinate each oxygen atom ( $\mu_3\text{–OH}$ ) in both brucite and portlandite. Of course, the  $\langle \text{M–O} \rangle$  bond distances differ depending upon whether the metal, M, is calcium or magnesium. These calculations are also an important test of the embedded-cluster approach in predicting RPF values and fractionation factors for oxygen isotopes.

## METHODS

**Isotope Conventions.** Isotopic exchange can be expressed by eq 1, for the reaction between liquid water ( $\text{H}_2\text{O}$ ) and either brucite or portlandite [ $\text{M}(\text{OH})_2$ ], where M represents either Ca(II) or Mg(II).



One can write an equilibrium expression for isotope exchange, eq 2, for the reaction above

$$K = \frac{(\text{H}_2^{16}\text{O})(\text{M}(\text{OH})_2)^{1/2}}{(\text{H}_2^{18}\text{O})(\text{M}(\text{OH})_2)^{1/2}} \quad (2)$$

This equilibrium constant is related to the measurable fractionation factor,  $\alpha$ , below. For a complete derivation showing the relationship between  $\alpha$  and  $K$ ; see the [Supporting Information](#).

**Electronic-Structure Methods and Models.** Density functional theory (DFT)<sup>23,24</sup> and Møller–Plesset second-order perturbation theory (MP2)<sup>25</sup> are used to calculate temperature-independent harmonic vibrational frequencies for embedded-cluster models of brucite and portlandite containing either  $^{16}\text{O}$  or  $^{18}\text{O}$ . Frequencies for water embedded in a cluster of other, explicit second-shell water molecules are compared with results using an isolated water in a perfect  $\text{H}_2\text{O}$  gas. RPF values are then computed from the strictly harmonic vibrational frequencies from each model, leading to estimates of the fractionation factors between each phase. Three molecular models were employed and are shown in [Figure 2b–d](#).

Electronic-structure calculations were carried out using the Gaussian 16, revision A.03 code.<sup>26</sup> All calculations employed tight optimization/SCF thresholds and ultrafine numerical integration grids. In general, exchange and correlation (XC) functionals of the generalized gradient approximation (GGA), BP86,<sup>27,28</sup> and PBE,<sup>29,30</sup> along with hybrid functionals

B3LYP<sup>28,31,32</sup> and PBE0<sup>33</sup> were employed. Second-order perturbation methods (MP2) to the Hartree–Fock energy were also used. The GGA, hybrid functionals, and MP2 methods were combined with the Pople triple- $\zeta$  basis set 6-311++G(2d, 2p), which includes diffuse functions, to represent oxygen and hydrogen. It has previously been shown that MP2 methods are well suited for the simulation of aqueous systems, because they include dispersion interactions that are not accounted for in DFT.<sup>34</sup> Furthermore, when combined with large basis sets (i.e., 6-311++G(2d,2p) or aug-cc-pVTZ), MP2 can be more reliable than DFT.<sup>34</sup>

The embedded-cluster model ([Figure 2b](#)) for water was constructed using CrystalMaker software by embedding one water molecule in four explicit water molecules and initially optimizing the entire structure with the B3LYP XC functional and the Pople double- $\zeta$  basis set 6-31G\*. A second calculation was performed on the cluster where the central water molecule in a tetrahedral cage of second-shell water molecules was reoptimized at B3LYP and 6-311++G(2d, 2p) basis on the oxygen and hydrogen atoms, while the second-shell waters were left in their 6-31G\* optimized positions but also being represented by the 6-311++G(2d, 2p) basis set. Similar calculations were also run on this cluster with a variety of XCs and basis sets, including combinations of B3LYP/cc-pVTZ, B3LYP/aug-cc-pVTZ, PBE0/6-311++G(2d, 2p), PBE/6-311++G(2d, 2p), BP86/6-311++G(2d, 2p), and MP2/6-311++G(2d, 2p). In most cases, the tetrahedral cluster was embedded in a dielectric medium (water,  $\epsilon_0 = 78.355300$ ,  $\epsilon_\infty = 1.777849$ ) using the polarizable continuum model (PCM).<sup>35</sup> In vacuo calculations were carried out for comparison.

Harmonic frequencies and RPF values were calculated for a similar embedded-cluster model of water to test the validity of the tetrahedral water model presented above and to examine the variation in the RPF as a function of the number of water molecules in the cluster. A cluster of 10 water molecules was first optimized in both the gas phase and then embedded in PCM at the B3LYP/6-31G\* level of theory and then reoptimized using the 6-311++G(2d, 2p) basis set (see [Supporting Information](#) for results). Finally, a series of calculations on a single gas-phase  $\text{H}_2\text{O}$  molecule at the MP2/6-311++G(2d, 2p), B3LYP/6-311++G(2d, 2p), /aug-cc-pVTZ, and PBE0/6-311++G(2d, 2p), levels were also performed (see [Figure 2a](#)), and these are similar to recent calculations of Asaduzzaman and Ganguly.<sup>8</sup> Calculated RPF values were compared to experimental measurements of oxygen-isotope RPF values from the  $\text{CO}_2$ -equilibration technique. The calculated frequencies for water were compared to the three molecular vibrational modes associated with bending/scissoring, symmetric stretching, and asymmetric stretching, determined by infrared spectroscopy.

Embedded-cluster models of the minerals brucite and portlandite were prepared using the Pauling-bond-strength-conserving termination method for mineral lattices. This method was described by Rustad et al.<sup>34,36</sup> and Colla et al.<sup>22</sup> The brucite cluster was taken from the crystal structure of Zigan and Rothbauer.<sup>37</sup> The portlandite structure was taken from the crystal structure of Busing and Levy.<sup>38</sup> Both structures were based upon neutron diffraction. A metal-hydroxide trimer was excised from the crystal structure, and the clipped bonds between the metal and oxygen of the outer shell were replaced with terminal atoms carrying point charges that equal the charge of the cation divided by its coordination number. In both brucite and portlandite models, the cation

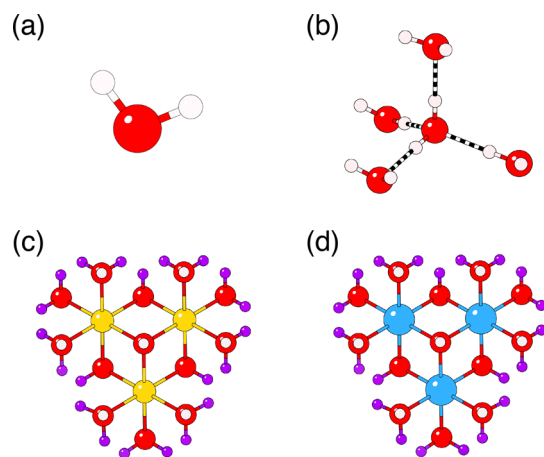


**Figure 2.** Molecular models used to represent both the metal-hydroxide mineral and the aqueous environments. (a)  $\text{H}_2\text{O}$  as a gas molecule. (b) Tetrahedral cluster of  $\text{H}_2\text{O}$  molecules, where dashed bonds represent hydrogen bonds. (c) Cluster of brucite as employed in the embedded-cluster calculations. (d) A corresponding cluster of portlandite. Red spheres are oxygen, white spheres are hydrogen, yellow spheres are magnesium, blue spheres are calcium, and purple spheres are fractional point charges to make an electrically neutral cluster.

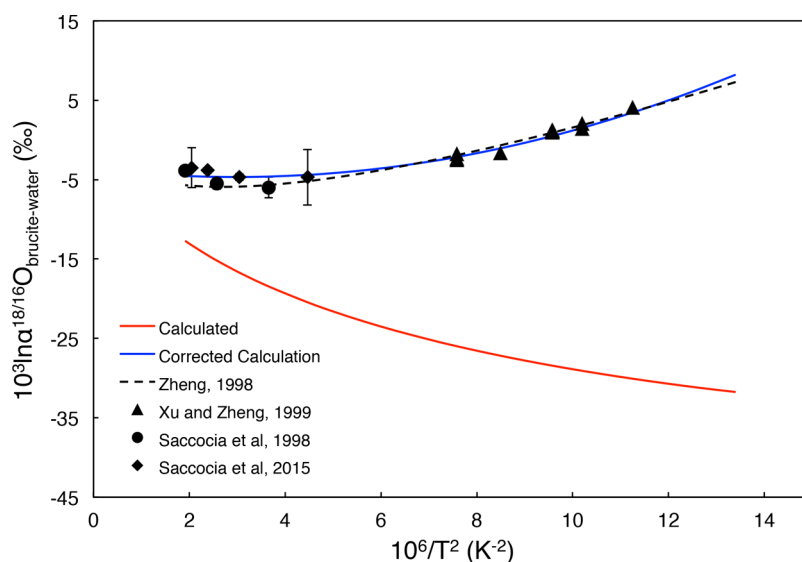


**Figure 3.** A plot of oxygen-isotope fractionation factor,  $10^3 \ln(\alpha)$ , as a function of temperature between brucite and water, including experiments of Saccoccia et al.<sup>14,15</sup> and Xu and Zheng.<sup>16</sup> The empirical predictions of Zheng<sup>13</sup> have also been included (dashed black line). Solid lines on the plot represent theoretical predictions from this study. Error bars are from Saccoccia et al.<sup>14,15</sup>

charge is 2+, and the coordination number is 6, equating to (+2/6) charge on each link atom to make a neutral cluster. The bond-strength-conserving method avoids terminating the cluster with integer charges, which can cause SCF convergence problems. Each cluster was centered on the tetrahedral oxygen site to be used in the optimization calculation and vibrational frequency analysis. The oxygen environment in brucite and portlandite makes a pseudoadamantane geometry due to the tetrahedral coordination of the oxygen site (see Figure 2c,d).

Both brucite- and portlandite-cluster models were initially optimized using the B3LYP functional with the 6-31G\* basis representing all atoms and with the PCM solvent model employed to help achieve electronic stability. Similar to the methods used to compute frequencies for the tetrahedral water cluster, the mineral clusters were then reoptimized by freezing all atoms except for the central hydroxide moiety, which was used to compute vibrational frequencies. The frozen lattice was represented by the 6-31G\* basis set, while the unfrozen hydroxide group, a  $\mu_3$ -OH site, was represented by the 6-311++G(2d,2p) basis set on both oxygen and hydrogen. The cluster was placed in a PCM cavity, as it was during the initial optimization, which was important. Computations of gas-phase clusters were also carried out for comparison. Comparison calculations were also performed on the brucite cluster, where the central  $\mu_3$ -OH and three metal atoms bound to the hydroxide were all allowed to move freely. The results of the calculations are tabulated in Table SI-2. The RPF for these calculations was only 0.0009 per mil lower than that of calculations provided in Table 3, where only the  $\mu_3$ -OH was allowed free motion.

A matrix of force constants was computed from the second partial derivative of the potential energy with respect to the displacements of two atoms in Cartesian coordinates. The force constants are then weighted by the atomic mass, and then, the frequencies for the heavy and light isotopes are calculated. The RPF values,  $\beta$ , are calculated from normal vibrational modes of optimized molecular models within the harmonic approximation using the same methods as in Colla et al.<sup>22</sup> As stated above, calculation of RPF values assumes a

strictly harmonic behavior. The value of  $\beta$  is related to partition functions in eq 3. In this equation,  $\beta$  values are estimated for ratios of the heavy (17.9991604) and light (15.9949146221) isotopes of oxygen, where  $Q_{(h,l)}$  are the vibrational partition coefficients for the heavy and light isotopes and  $u_{(h,l)i} = hc\omega_{(h,l)i}/k_B T$ , where  $h$  is Planck's constant,  $c$  is the speed of light in a vacuum,  $\omega$  corresponds to the vibrational frequency of either the light or heavy isotope in a molecular environment, and  $k_B T$  is a Boltzmann factor.<sup>1</sup>

$$\beta = \left( \frac{Q_h}{Q_l} \right) = \prod_i^{3N} \frac{u_{h_i} e^{-u_{h_i}/2}}{u_{l_i} (1 - e^{-u_{h_i}})} \frac{1 - e^{-u_{l_i}}}{e^{-u_{l_i}/2}} \quad (3)$$

For embedded-cluster models that are intended to represent solid mineral lattices, the number of vibrational degrees of freedom is the full  $3N$ , where  $N$  is the number of atoms being considered in the calculation; rotations and translations are nonexistent. For a molecule in the gas or liquid phase, there are  $3N$  vibrational, translational, and rotational degrees of freedom, with  $3N - 6$  vibrational modes for a nonlinear molecule (e.g.,  $H_2O$ ) and  $3N - 5$  modes for a linear molecule (e.g.,  $CO_2$ ).<sup>39</sup> Contributions from electronic degrees of freedom to the harmonic partition function are not accounted for. The Born–Oppenheimer approximation<sup>40</sup> is invoked here where the electronic structure of a molecule is independent of the nuclear isotopes.

We calculate the equilibrium constant,  $K$ , of the isotopic exchange reaction (eq 1) using the RPF formulation that was introduced by Urey,<sup>1</sup> exploiting the Teller–Redlich product rule that leads to an expression of  $K$  in terms of the  $\beta$  factors (eq 4). An important assumption behind this product rule is that the vibrational modes can be treated harmonically. Asaduzamann and Ganguly<sup>8</sup> have discussed why the harmonic approximation should work for isotopic exchange reactions, and the interested reader is referred to that paper for discussion. Positive values indicate an enrichment of the heavy isotope in the numerator, and negative values indicate depletion of the heavy isotope in the numerator.

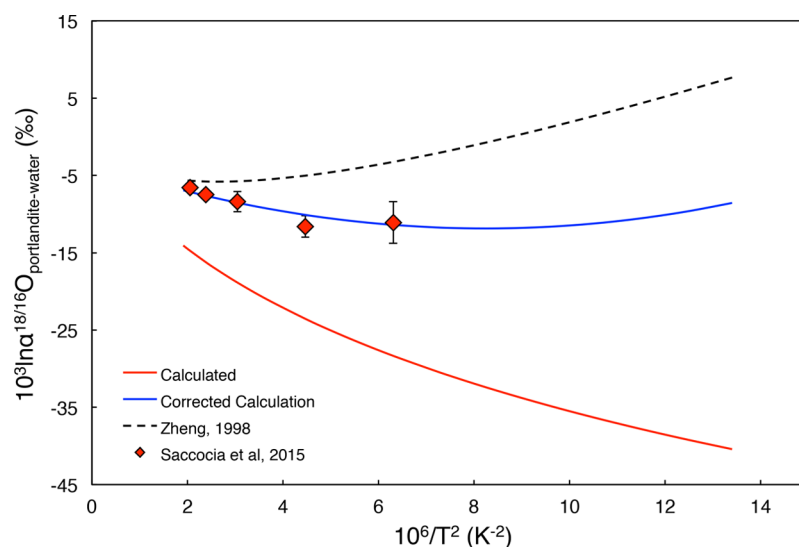


**Figure 4.** Plot of the fractionation factor,  $10^3 \ln(\alpha)$ , between portlandite and water as a function of temperature, including the experiments of Saccocia et al.<sup>14</sup> The empirical predictions of Zheng<sup>13</sup> have also been included (dashed black line). Solid lines on the plot represent theoretical predictions from this study. Error bars are from Saccocia et al.<sup>14</sup>

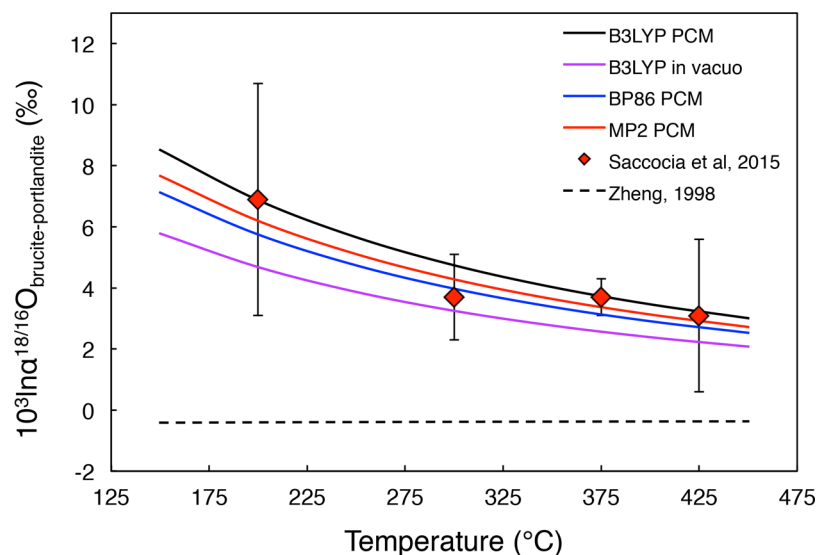


**Figure 5.** Predicted isotopic fractionation factor,  $10^3 \ln(\alpha)$ , between brucite and portlandite as a function of temperature (solid lines), compared to experiments of Saccocia et al.<sup>14</sup> (red diamonds), and empirical predictions of the fractionation by Zheng<sup>13</sup> (dashed line). Error bars are taken from Saccocia et al.<sup>14</sup>

$$K_{\text{mineral water}}^{\text{calculated}} = \left( \frac{(\beta_{\text{mineral}})^{1/2}}{\beta_{\text{water}}} \right) \quad (4)$$

The relationship between the experimentally determined fractionation factor,  $\alpha$ , and the equilibrium constant for isotope exchange is given by eq 5 (see Supporting Information).

$$K_{\text{mineral water}}^{\text{calculated}} = \alpha \quad (5)$$

**Increment Method.** Semiempirical mineral–water predictions of Zheng<sup>13</sup> were calculated using eq 6. (See dashed black functions in Figures 3 and 4).

$$10^3 \ln \alpha = \frac{A \cdot 10^6}{T^2} + \frac{B \cdot 10^3}{T} + C \quad (6)$$

Where  $A$ ,  $B$ , and  $C$  are empirical constants determined by polynomial fits to the fractionation data produced by the modified increment method. Eq 6 has both a  $1/T$  and  $1/T^2$  dependence, which is derived from the low- and high-temperature approximations to Urey's equations (see Criss<sup>41</sup> for derivation).

Predictions of brucite–portlandite fractionation based on the increment method were calculated using eq 7. In this equation,  $10^3 \ln(\beta_{\text{mineral}})$  was calculated via eq 8,  $I^{-18}\text{O}$  is the mineral index (See Zheng<sup>9</sup> for explanation),  $D$  is a low-temperature correction term defined by eq 9, and  $10^3 \ln(\beta_{\text{reference}})$  is the  $\beta$ -factor for a reference mineral, in this case, quartz at 298.15 K taken from Clayton et al.<sup>42</sup>  $\Delta E$  in eq 9 is the isotopic partitioning energy for low temperatures,  $R$  is the gas constant, and  $T$  is the absolute temperature in Kelvin. The isotopic partitioning energy is assumed to be a constant at  $1000 \text{ J mol}^{-1}$ .<sup>12</sup>

$$10^3 \ln \alpha_{\text{brucite-portlandite}} = 10^3 \ln \beta_{\text{brucite}} - 10^3 \ln \beta_{\text{portlandite}} \quad (7)$$

$$10^3 \ln \beta_{\text{mineral}} = I^{-18} O_{\text{mineral}} \cdot D \cdot 10^3 \ln \beta_{\text{reference}} \quad (8)$$

$$D = e^{\left(\frac{\Delta E_{I-18} O_{\text{mineral}}}{RT}\right)} \quad (9)$$

## RESULTS

The predicted temperature dependencies of the oxygen-isotope-exchange reactions are shown in Figures 3, 4, and 5 for brucite–water, portlandite–water, and brucite–portlandite systems, respectively.

**RPFR Values.** Calculated RPFR values for water, brucite, and portlandite are presented in Tables 1–4. As discussed

**Table 1.**  $O^{18/16}$  Reduced-Partition-Function Ratios (RPFR) for Water in Vacuo at 298.15 K

method/basis set/solvation	$\beta$ (RPFR)
<b>B3LYP</b>	
6-311++G(2d,2p)(O,H)	1.066302
aug-cc-pVTZ(O,H)	1.065806
<b>MP2</b>	
6-311++G(2d,2p)(O,H)	1.067044
<b>PBE0</b>	
6-311++G(2d,2p)(O,H)	1.067383

**Table 2.**  $O^{18/16}$  RPFR Values for Tetrahedral Water Cluster at 298.15 K

method/basis set/solvation	$\beta$ (RPFR)
<b>B3LYP</b>	
6-31G*/PCM	1.080366
cc-pVTZ/PCM	1.078510
aug-cc-pVTZ/PCM	1.078257
6-311++G(2d,2p)(O,H)/PCM	1.079094
<b>PBE0</b>	
6-311++G(2d,2p)(O,H)/PCM	1.079536
<b>PBE</b>	
6-311++G(2d,2p)(O,H)/PCM	1.075908
<b>BP86</b>	
6-311++G(2d,2p)(O,H)/PCM	1.075622
<b>MP2</b>	
6-311++G(2d,2p)(O,H)/PCM	1.080291
6-311++G(2d,2p)(O,H)/(all atoms active)/in vacuo	1.081082

above in the Methods section, two models for water were considered: (i) a single  $H_2O$  gas molecule (Figure 2a and Table 1), and (ii) a tetrahedral water cluster (Figure 2b and Table 2). The RPFR values of these separate models differ by about  $\sim 12$  per mil, with the RPFR values calculated from the tetrahedral water being larger. Comparisons between calculated and measured bond distances and vibrational frequencies are tabulated in Tables 5, SI-4, -5, and -6.

The RPFR values that were calculated using electronic-structure methods and a variety of XC functionals for DFT, basis sets, and continuum-solvent methods (e.g., PCM) are in good agreement with each other. MP2 methods tend to also agree well with predictions at the DFT level using hybrid functionals. On average, calculations carried out using PCM result in RPFR values  $\sim 1$  per mil lower than calculations in vacuo, consistent with previous calculations on other

**Table 3.**  $O^{18/16}$  RPFR Values for the Brucite Trimer Cluster at 298.15 K

method/basis set/solvation	$\beta$ (RPFR)
<b>B3LYP</b>	
6-31G*(O,H,Mg)/PCM	1.071453
6-311++G(2d,2p)(O,H)/6-31G*(lattice)/PCM	1.070614
6-311++G(2d,2p)(O,H)/6-31G*(lattice)/in vacuo	1.071535
<b>PBE0</b>	
6-311++G(2d,2p)(O,H)/6-31G*(lattice)/PCM	1.071545
<b>PBE</b>	
6-311++G(2d,2p)(O,H)/6-31G*(lattice)/PCM	1.067871
<b>BP86</b>	
6-311++G(2d,2p)(O,H)/6-31G*(lattice)/PCM	1.067537
<b>MP2</b>	
6-311++G(2d,2p)(O,H)/6-31G*(lattice)/PCM	1.072118
6-311++G(2d,2p)(O,H)/6-31G*(lattice)/in vacuo	1.073027

**Table 4.**  $O^{18/16}$  RPFR Values for the Portlandite Trimer Cluster at 298.15 K

method/basis set/solvation	$\beta$ (RPFR)
<b>B3LYP</b>	
6-311++G(2d,2p)(O,H)/6-31G*(lattice)/PCM	1.055091
6-311++G(2d,2p)(O,H)/6-31G*(lattice)/in vacuo	1.059782
<b>PBE0</b>	
6-311++G(2d,2p)(O,H)/6-31G*(lattice)/PCM	1.056422
<b>PBE</b>	
6-311++G(2d,2p)(O,H)/6-31G*(lattice)/PCM	1.052927
<b>BP86</b>	
6-311++G(2d,2p)(O,H)/6-31G*(lattice)/PCM	1.053017
<b>MP2</b>	
6-311++G(2d,2p)(O,H)/6-31G*(lattice)/PCM	1.056422

**Table 5.** Calculated and Measured Average  $\langle O-H \rangle$ ,  $\langle Mg-O \rangle$ , and  $\langle Ca-O \rangle$  Bond Distances for Brucite and Portlandite<sup>a</sup>

	calculated (Å)	measured (Å)
brucite $\langle O-H \rangle$	0.958	0.995 <sup>b</sup>
brucite $\langle Mg-O \rangle$	2.102	2.099 <sup>b</sup>
portlandite $\langle O-H \rangle$	0.955	0.935 <sup>c</sup>
portlandite $\langle Ca-O \rangle$	2.414	2.370 <sup>c</sup>

<sup>a</sup>Measured distances are from neutron diffraction. <sup>b</sup>Zigan and Rothbauer.<sup>37</sup> <sup>c</sup>Busy and Levy.<sup>38</sup>

clusters.<sup>22,34</sup> In all cases, using a lower number of basis functions did not have a large effect on the calculated RPFR. Consider, for example, calculations performed using the B3LYP functional on the brucite model. Using the less expensive 6-31G\* basis set on all atoms causes only a  $\sim 1$  per mil difference in the computed RPFR value (see Table 3) when compared to the more expensive 6-311++G(2d, 2p) basis set. Previous workers have shown that RPFR values are expected to change in aqueous systems as the number of basis functions per water molecule increases, but the change is not large for the systems described here.<sup>34</sup>

A larger discrepancy between computed RPFR values comes from the choice of XC functionals, as has also been noted before.<sup>22</sup> For example, brucite RPFR values predicted using the same number of basis functions and solvation models have a  $\sim 4$  per mil difference between hybrid methods and GGA methods. Such hybrid functionals mix some Hartree–Fock exact-exchange terms into the exchange and correlation energy.

The hybrid methods are ~4 per mil heavier. The MP2 methods, in contrast, produce results that agree well with hybrid DFT methods but are consistently ~1.3 per mil heavier than hybrid DFT methods.

Calculated  $^{18/16}\text{O}$  RPF values for water, either as a tetrahedral cluster or as a single molecule in the gas phase, deviate from the measured RPF values. The measurements were via the  $\text{CO}_2$ -equilibration method by O'Neil and Adami.<sup>43</sup> The best agreement with the  $\text{CO}_2$ -equilibration technique comes from the calculated RPF of a single  $\text{H}_2\text{O}$  molecule. At 30 °C, the experimentally determined RPF as  $10^3 \ln(\beta)$  is 69.59, while calculations using MP2 and the 6-311++G(2d,2p) basis set for water yield 68.65.

**Bond Distances.** Calculated  $\langle\text{O}-\text{H}\rangle$ ,  $\langle\text{Mg}-\text{O}\rangle$ , and  $\langle\text{Ca}-\text{O}\rangle$  distances are compared in Table 5 to measured bond distances using neutron-diffraction methods for both brucite and portlandite. Metal-oxide bond distances were analyzed from the metal site to the particular oxygen site that was used to compute the RPF values. The calculated  $\langle\text{O}-\text{H}\rangle$  bond distance of brucite is on average 0.037 Å shorter than that determined via neutron diffraction, while the calculated  $\langle\text{O}-\text{H}\rangle$  bond distance of portlandite is 0.02 Å higher than the experimental measurement. Calculated metal-oxide bond distances for both portlandite and brucite are, on average, higher than measurements, which is consistent with previous calculations at similar levels of theory, using similar embedded-cluster models.<sup>22</sup> Calculated brucite  $\langle\text{Mg}-\text{O}\rangle$  bond distances are 0.003 Å longer than measured distances, and calculated  $\langle\text{Ca}-\text{O}\rangle$  bond distances in portlandite are 0.044 Å longer than measured values.

**Vibrational Frequencies.** Calculated frequencies are generally higher than measured frequencies. For water molecules, calculated average vibrational frequencies for the two separate models (a single gaseous  $\text{H}_2\text{O}$  and a cluster of waters) are tabulated and compared to measured frequencies of liquid water in Table SI-4. There is a close agreement between the frequencies calculated for the tetrahedral water model and frequencies measured spectroscopically. The bending and symmetric-stretching modes of the tetrahedral model are slightly overestimated, while the asymmetric-stretching mode is very close to the measured frequency. Calculated frequencies using an isolated  $\text{H}_2\text{O}$  gas molecule are generally higher than experiment. The bending mode compares well with experiment, but the two stretching mode frequencies are grossly overestimated.

For the solids, calculated frequencies of the OH-stretching mode in brucite and portlandite are reported in Tables SI-5 and -6. On average, calculated OH-stretching modes in minerals brucite and portlandite are ~200–300  $\text{cm}^{-1}$  higher than observed by vibrational spectroscopy. This difference is typical (see below).

**Fractionation Factors.** Calculated fractionation factors,  $\alpha$  values, are computed for the brucite–water, portlandite–water, and brucite–portlandite systems over a wide temperature range in order to compare with experiments by Saccocia et al.<sup>14</sup> and Xu and Zheng.<sup>16</sup> Calculated fractionation factors underestimate the experimentally observed values for any reaction involving a water molecule, such as the brucite–water and portlandite–water systems, which are shown as red lines in Figures 3 and 4. In general, calculations using DFT and MP2 methods overlie one another when predicting mineral–water fractionations. For the sake of simplicity, we only plot fractionation factors predicted using the MP2 method in

Figures 3 and 4. DFT and MP2 methods predict fractionation factors within the reported errors of the experimental results for the brucite–portlandite system and agree well with the experimental trend (see Figure 5).

## DISCUSSION

**Vibrational Frequencies.** Vibrational frequencies computed from DFT and MP2, in general, are higher than those measured spectroscopically (See Tables SI-5 and 6). Calculated frequencies for OH-stretching modes in brucite and portlandite, on average, are overestimated by up to ~300  $\text{cm}^{-1}$ . The overestimation of harmonic frequencies by ab initio methods is commonly observed and was discussed by Scott and Radom<sup>44</sup> and has been attributed to anharmonic effects that are not accounted in traditional ab initio calculations. Other sources of error include incomplete implementation of electron correlation in the method and finite basis sets (Scott and Radom<sup>44</sup>).

**Oxygen-Isotope Fractionation between Brucite and Water.** Calculated fractionations from this study do not agree with experimental data in the temperature range of 25–450 °C. We therefore have applied a correction to our calculated fractionation factors so that it agrees with experiments, following the lead of Méheut et al.<sup>5</sup> Eq 10 is a correction for brucite and water, where  $x = 10^6/T^2$ .

$$10^3[\ln \alpha_{\text{exp}}^{18/16}\text{O}_{\text{portlandite-water}} - \ln a_{\text{calc}}^{18/16}\text{O}_{\text{portlandite-water}}] = 0.2042x + 3.6344 \quad (10)$$

**Oxygen-Isotope Fractionation between Portlandite and Water.** The fractionation factors predicted from electronic-structure calculations for the portlandite–water system are shown in Figure 4. Similar to the predictions of brucite–water fractionations, a correction was applied to align the calculated fractionation factors with experiments. Corrections to the calculated values are plotted in Figure 4, and the equation itself is

$$10^3[\ln \alpha_{\text{exp}}^{18/16}\text{O}_{\text{portlandite-water}} - \ln a_{\text{calc}}^{18/16}\text{O}_{\text{portlandite-water}}] = 2.0536x + 3.7992 \quad (11)$$

where  $x = 10^6/T^2$ .

Also shown in the figure are predictions using the method of Zheng.<sup>13</sup> These semiempirical methods overestimate the amount of isotopic fractionation and predict a similar fractionation as for the brucite–water system (see Figure 4) and a similar temperature dependence. The semiempirical methods of Zheng<sup>13</sup> predict fractionations that are significantly higher than the experimental results between 125 and 425 °C, which is perhaps unsurprising, since the  $\langle\text{Si}-\text{O}\rangle$  bond distance, which is an essential reference for the increment method, is ~1 Å, shorter than the  $\langle\text{Ca}-\text{O}\rangle$  bond distance of ~2.4 Å. Stated differently, the semiempirical method is poorly parametrized for portlandite.

Magnitudes of fractionation differ as well, and unsurprisingly so, because of the differences in  $\langle\text{M}-\text{O}\rangle$  bond strengths. The observed fractionation factors from Saccocia et al.<sup>14</sup> for portlandite–water fractionation are significantly lower and isotopically lighter than the brucite–water system, indicating that portlandite is significantly depleted in  $^{18}\text{O}$  relative to brucite. Correspondingly, the  $\langle\text{Ca}-\text{O}\rangle$  bond distance is ~0.3 Å longer than the  $\langle\text{Mg}-\text{O}\rangle$  bond distance, and therefore, isotopic exchange is energetically favorable.



**Oxygen-Isotope Fractionation between Brucite and Portlandite.** Error from choice of a water model can be eliminated by comparing isotopic exchange between solids only. Fractionation factors between minerals brucite and portlandite are plotted over the temperature range 150–450 °C in Figure 5, along with experimental data of Saccocia et al.<sup>14</sup> Also calculated and plotted are the empirical predictions of Zheng.<sup>13</sup> Results of the predictions carried out in this study are tabulated in Table 6, along with the data points from

**Table 6. Predicted Fractionation Factors, as  $10^3 \ln(\alpha_{\text{brucite-portlandite}})$ , in per mil, between Brucite and Portlandite<sup>a</sup>**

method	200 °C	300 °C	375 °C	425 °C
B3LYP PCM	6.87	4.74	3.34	2.89
B3LYP in vacuo	4.68	3.24	2.56	2.22
BP86 PCM	5.74	3.97	3.13	2.71
MP2 PCM	6.19	4.28	3.37	2.91
Saccocia et al. (2015)	+6.9 (±3.8)	+3.7 (±1.4)	+3.7 (±0.6)	+3.1 (±2.5)

<sup>a</sup>Using various XC functionals and the 6-311++G(2d,2p) basis set on the mobile  $\mu_3$ -OH and 6-31G\* on the frozen lattice.

Saccocia et al.<sup>14</sup> Predictions of specific fractionation factors are reported in Table 6 and are within reported uncertainties of the experimental values. The predicted fractionation over the temperature range of 150–450 °C also agrees well with the experimental trend of the data. The calculations consistently predict brucite to be enriched in <sup>18</sup>O relative to portlandite. The semiempirical method fails to recover the fractionation from 150 to 450 °C and predicts virtually no oxygen-isotopic fractionation between the two minerals. The semiempirical method predicts a very small enrichment of portlandite in <sup>18</sup>O.

**Discrepancy between Theory and Experiment.** Calculated fractionation factors, before correction in the brucite–water system, are lighter than experimental determinations by anywhere from 30 per mil at low temperatures to 8 per mil at high temperatures. In the portlandite–water system, calculated fractionations range from 17 per mil at 125 °C to 8 per mil at 425 °C, with the solid being depleted in <sup>18</sup>O. The differences reported here are consistent in magnitude but not direction, with differences reported by Méheut et al.<sup>5</sup> for D/H fractionation between brucite and water. Méheut et al.<sup>5</sup> attributed the discrepancy between experiments and calculations to neglect of anharmonic effects to the vibrational modes.

The discrepancy reported here for any reaction involving water probably also arises from anharmonic effects in the vibrational modes of water. We reach this conclusion because the calculated fractionation factors between brucite and portlandite agree well with experiments, indicating that the discrepancy between mineral–water fractionations must arise from error in the calculation of water vibrational frequencies. Also pointed out by Méheut et al.<sup>5</sup> is the work of Richet et al.,<sup>2</sup> who show that the anharmonic contribution to the  $\beta$ -factor of water is 125 per mil at 25 °C. Similarly, Reynard and Caracas<sup>6</sup> find that the anharmonic contribution to the  $\beta$ -factor at 275 and 1000 K are 60 and 20 per mil, respectively, for OH stretching in brucite, much smaller than for water.

**Water Model.** Best agreement was achieved using a single H<sub>2</sub>O molecule rather than a larger model of several bonded waters to approximate the bulk water environment. Previous

workers have also reported this finding.<sup>4,5,8</sup> Predictions using tetrahedrally coordinated water clusters are distinct and do not reproduce experimental results at either low or high temperatures. Using a single water molecule, predictions of fractionations are insensitive to level of theory, at least for the three different functionals and MP2 levels investigated here. The results for different levels of theory would virtually overlay one another in Figures 3 and 4, even if they are offset from the experimental results.

**Other Work.** A recent paper by Asaduzzaman and Ganguly<sup>8</sup> guided our study and employed similar techniques to calculate hydrogen-isotope fractionations in the epidote–H<sub>2</sub> and epidote–water systems. They exploited the efficient optimization algorithms that are available in plane-wave DFT codes to first relax the epidote lattice. With this fully relaxed structure, they then employed cluster techniques (similar to those we use here) to calculate vibrational frequencies for an epidote-like cluster. In the cluster calculation of Asaduzzaman and Ganguly, they used the B3LYP exchange-correlation functional and a Pople basis set 6-311G+(p,d), which includes polarization and diffuse functions, similar to some of those we employ in this study but with small differences in the assignment of diffuse functions to hydrogens. One discrepancy between this study and that of Asaduzzaman and Ganguly is in the treatment of the molecular cluster. Because Asaduzzaman and Ganguly carved out a neutral stoichiometric cluster from the epidote lattice, it was not necessary to neutralize the cluster with point charges as we had to do here for metal-hydroxide solids.

The calculations in the brucite–portlandite system presented here complement those of Blanchard et al.<sup>7</sup> who noted similar discrepancies between measured isotopic fractionations and those predicted using the increment method. Blanchard et al.<sup>7,45</sup> compared their calculations of oxygen-isotope RPF values for goethite and previous RPF calculations of hematite and corundum to the calculations of Zheng.<sup>9,13</sup> The origins of the discrepancy between predictions based upon the quantum methods and those from the increment method lie in the use of a reference mineral  $\beta$ -factor from quartz at 298.15 K (from Clayton et al.<sup>42</sup>) for minerals like the metal-hydroxide solids.

## CONCLUSIONS

The equilibrium fractionation of oxygen isotopes between water and two simple metal-hydroxide minerals, brucite and portlandite, was predicted using electronic-structure methods. The calculations recover the experimental data only after application of a correction term if the reaction involved water. It is likely that the error in prediction of these fractionation factors arises due to anharmonic contributions to the vibrational modes of water that propagate through the calculation of RPF values and therefore fractionation factors. Future calculations of mineral–water fractionations must account for anharmonic effects. The calculations of RPF values are robust to choice of basis set and functional over a wide range, and anhydrous solid–solid fractionations required no corrections.

## ASSOCIATED CONTENT

### Supporting Information

The Supporting Information is available free of charge on the ACS Publications website at DOI: 10.1021/acsearthspacechem.9b00020.

Supporting calculations, xyz structures of optimized molecular models used in the calculation of vibrational frequencies, description of how to use the Python code (PDF)

Python code for computing oxygen-isotope RPF values (PDF)

## AUTHOR INFORMATION

### Corresponding Author

\*E-mail: [cacolla@lbl.gov](mailto:cacolla@lbl.gov). (C.A.C.)

### ORCID

Christopher A. Colla: 0000-0002-2095-3752

William H. Casey: 0000-0002-3275-6465

### Author Contributions

C.A.C. conceived of the problem and performed the calculations with assistance by W.H.C., and both C.A.C. and W.H.C. wrote the manuscript. All authors have given approval to the final version of the manuscript.

### Notes

The authors declare no competing financial interest.

## ACKNOWLEDGMENTS

The authors would like to thank Professor Sumit Chakraborty for editorial handling of the manuscript. The authors would also like to thank three perceptive reviewers. Particular thanks is due to one particular referee who uncovered important errors in the original work. The authors are indebted to Professor Jibamitra Ganguly for generous discussion and suggestions. This work was supported by the U.S. Department of Energy, Office of Basic Energy Sciences, Chemical Sciences, Geosciences, and Biosciences Division, through its Geoscience program at Lawrence Berkeley National Laboratory under Contract DE-AC02-05CH11231. W.H.C. acknowledges support from the U.S. Department of Energy Office of Basic Energy Sciences, Chemical Sciences, Geosciences, and Biosciences Division, via grant DE-FG0205SER15693.

## ABBREVIATIONS

XC, exchange and correlation; RPF, reduced-partition-function ratio; DFT, density functional theory; MP2, Møller–Plesset second-order perturbation theory; PBS, Pauling bond strength

## REFERENCES

- (1) Urey, H. C. Thermodynamic properties of isotopic substances. *J. Chem. Soc.* **1947**, 562–581.
- (2) Richet, P.; Bottinga, Y.; Javoy, M. A review of hydrogen, carbon, nitrogen, oxygen, sulphur, and chlorine stable isotope fractionation among gaseous molecules. *Annu. Rev. Earth Planet. Sci.* **1977**, *5*, 65–10.
- (3) Chacko, T.; Cole, D. R.; Horita, J. Equilibrium oxygen, hydrogen and carbon isotope fractionation factors applicable to geologic systems. *Rev. Mineral. Geochem.* **2001**, *43*, 1–81.
- (4) Méheut, M.; Lazzeri, M.; Balan, E.; Mauri, F. Equilibrium isotopic fractionation in the kaolinite, quartz, water system: Prediction from first-principles density-functional theory. *Geochim. Cosmochim. Acta* **2007**, *71*, 3170–3181.
- (5) Méheut, M.; Lazzeri, M.; Balan, E.; Mauri, F. First-principles calculation of H/D isotopic fractionation between hydrous minerals and water. *Geochim. Cosmochim. Acta* **2010**, *74*, 3874–3882.
- (6) Reynard, B.; Caracas, R. D/H isotopic fractionation between brucite  $\text{Mg}(\text{OH})_2$  and water from first-principles vibrational modeling. *Chem. Geol.* **2009**, *262*, 159–168.
- (7) Blanchard, M.; Dauphas, N.; Hu, M. Y.; Roskosz, M.; Alp, E. E.; Golden, D. C.; Sio, C. K.; Tissot, F. L. H.; Zhao, J.; Gao, L.; Morris, R. V.; Fornace, M.; Floris, A.; Lazzeri, M.; Balan, E. Reduced partition function ratios of iron and oxygen in goethite. *Geochim. Cosmochim. Acta* **2015**, *151*, 19–33.
- (8) Asaduzzaman, A.; Ganguly, J. Hydrogen isotope fractionation in the epidote-hydrogen and epidote-water systems: theoretical study and implications. *Earth and Space Chem.* **2018**, *2*, 1029–1034.
- (9) Zheng, Y.-F. Calculation of oxygen isotope fractionation in metal oxides. *Geochim. Cosmochim. Acta* **1991**, *55*, 2299–2307.
- (10) Zheng, Y. F. Calculation of oxygen isotope fractionation in anhydrous silicate minerals. *Geochim. Cosmochim. Acta* **1993**, *57*, 1079–1091.
- (11) Zheng, Y. F. Calculation of oxygen isotope fractionation in hydroxyl-bearing silicates. *Earth Planet. Sci. Lett.* **1993**, *120*, 247–263.
- (12) Zheng, Y. F. Oxygen isotope fractionations involving apatites: Application to paleotemperature determination. *Chem. Geol.* **1996**, *127*, 177–187.
- (13) Zheng, Y. F. Oxygen isotope fractionation between hydroxide minerals and water. *Phys. Chem. Miner.* **1998**, *25*, 213–221.
- (14) Saccocia, P. J.; Seewald, J. S.; Shanks III, W. C. Oxygen isotope fractionation in the portlandite-water and brucite-water systems from 125 to 450°C, 50 MPa. *Geochim. Cosmochim. Acta* **2015**, *169*, 137–151.
- (15) Saccocia, P. J.; Seewald, J. S.; Shanks III, W. C. Hydrogen and oxygen isotope fractionation between brucite and aqueous NaCl solutions from 250 to 450°C. *Geochim. Cosmochim. Acta* **1998**, *62*, 485–492.
- (16) Xu, B. L.; Zheng, Y. F. Experimental studies of oxygen and hydrogen isotope fractionations between precipitated brucite and water at low temperatures. *Geochim. Cosmochim. Acta* **1999**, *63*, 2009–2018.
- (17) Horita, J.; Driesner, T.; Cole, D. R. Pressure effect on hydrogen isotope fractionation between brucite and water at elevated temperatures. *Science* **1999**, *286*, 1545–1547.
- (18) Horita, J.; Driesner, T.; Cole, D. R. Hydrogen isotope fractionation in the systems brucite-water  $\pm$  NaCl to elevated temperatures and pressures: Implications for the isotopic property of NaCl fluids under geologic conditions. *Geochim. Cosmochim. Acta* **2018**, *235*, 140–152.
- (19) Wimpenny, J.; Colla, C. A.; Yin, Q. Z.; Rustad, J. R.; Casey, W. H. Investigating the behavior of Mg isotopes during the formation of clay minerals. *Geochim. Cosmochim. Acta* **2014**, *128*, 178–194.
- (20) Li, W.; Beard, B. L.; Li, C.; Johnson, C. M. Magnesium isotope fractionation between brucite  $[\text{Mg}(\text{OH})_2]$  and Mg aqueous species: Implications for silicate weathering and biogeochemical processes. *Earth Planet. Sci. Lett.* **2014**, *394*, 82–93.
- (21) Ryu, J. S.; Vigier, N.; Decarreau, A.; Lee, S. W.; Lee, K. S.; Song, H.; Petit, S. Experimental investigation of Mg isotope fractionation during mineral dissolution and clay formation. *Chem. Geol.* **2016**, *445*, 135–145.
- (22) Colla, C. A.; Casey, W. H.; Ohlin, C. A. Computational prediction of Mg-isotope fractionation between aqueous  $[\text{Mg}(\text{OH})_6]^{2+}$  and brucite. *Geochim. Cosmochim. Acta* **2018**, *227*, 64–74.
- (23) Hohenberg, P.; Kohn, W. Inhomogeneous electron gas. *Phys. Rev.* **1964**, *136*, B864–B871.
- (24) Kohn, W.; Sham, L. J. Self-consistent equations including exchange and correlation effects. *Phys. Rev.* **1965**, *140*, A1133–A1138.
- (25) Møller, C. H. R.; Plesset, M. S. Note on an approximation treatment for many-electron systems. *Phys. Rev.* **1934**, *46*, 618–622.
- (26) Frisch, M. J.; Trucks, G. W.; Schlegel, H. B.; Scuseria, G. E.; Robb, M. A.; Cheeseman, J. R.; Scalmani, G.; Barone, V.; Petersson, G. A.; Nakatsuji, H.; Li, X.; Caricato, M.; Marenich, A. V.; Bloino, J.; Janesko, B. G.; Gomperts, R.; Mennucci, B.; Hratchian, H. P.; Ortiz, J. V.; Izmaylov, A. F.; Sonnenberg, J. L.; Williams-Young, D.; Ding, F.; Lipparini, F.; Egidi, F.; Goings, J.; Peng, B.; Petrone, A.; Henderson, T.; Ranasinghe, D.; Zakrzewski, V. G.; Gao, J.; Rega, N.; Zheng, G.; Liang, W.; Hada, M.; Ehara, M.; Toyota, K.; Fukuda, R.; Hasegawa, J.; Ishida, M.; Nakajima, T.; Honda, Y.; Kitao, O.; Nakai, H.; Vreven, T.;

Throssell, K.; Montgomery, J. A., Jr.; Peralta, J. E.; Oligaro, F.; Bearpark, M. J.; Heyd, J. J.; Brothers, E. N.; Kudin, K. N.; Staroverov, V. N.; Keith, T. A.; Kobayashi, R.; Normand, J.; Ragavachari, K.; Rendell, A. P.; Burant, J. C.; Iyengar, S. S.; Tomasi, J.; Cossi, M.; Millam, J. M.; Klene, M.; Adamo, C.; Cammi, R.; Ochterski, J. W.; Martin, R. L.; Morokuma, K.; Farkas, O.; Foresman, J. B.; Fox, D. J. *Gaussian 16*, revision A.03; Gaussian, Inc.: Wallingford, CT, 2016.

(27) Perdew, J. P. Density-functional approximation for the correlation-energy of the inhomogeneous electron-gas. *Phys. Rev. B: Condens. Matter Mater. Phys.* **1986**, *33*, 8822–8824.

(28) Becke, A. D. Density-functional exchange-energy approximation with correct asymptotic behavior. *Phys. Rev. A: At, Mol, Opt. Phys.* **1988**, *38*, 3098–3100.

(29) Perdew, J. P.; Burke, K.; Ernzerhof, M. Generalized gradient approximation made simple. *Phys. Rev. Lett.* **1996**, *77*, 3865–3868.

(30) Perdew, J. P.; Ernzerhof, M.; Burke, K. Rationale for mixing exact exchange with density functional approximations. *J. Chem. Phys.* **1996**, *105*, 9982–9985.

(31) Becke, A. D. Density-functional thermochemistry. III. The role of exact exchange. *J. Chem. Phys.* **1993**, *98*, 5648–5652.

(32) Lee, C. T.; Yang, W. T.; Parr, R. G. Development of the collesalvetti correlation-energy formula into a functional of the electron-density. *Phys. Rev. B: Condens. Matter Mater. Phys.* **1988**, *37*, 785–789.

(33) Adamo, C.; Barone, V. Toward reliable density functional methods without adjustable parameters: the PBE0 model. *J. Chem. Phys.* **1999**, *110*, 6158–6159.

(34) Rustad, J. R.; Casey, W. H.; Yin, Q. Y.; Bylaska, E. J.; Felmy, A. R.; Bogatko, S. A.; Jackson, V. E.; Dixon, D. A. Isotopic fractionation of  $Mg^{2+}(aq)$ ,  $Ca^{2+}(aq)$ , and  $Fe^{2+}(aq)$  with carbonate minerals. *Geochim. Cosmochim. Acta* **2010**, *74*, 6301–6323.

(35) Tomasi, J.; Mennucci, B.; Cammi, R. Quantum mechanical continuum solvation models. *Chem. Rev.* **2005**, *105*, 2999–3093.

(36) Rustad, J. R.; Nelmes, S. L.; Jackson, V. E.; Dixon, D. A. Quantum-chemical calculations of carbon-isotope fractionation in  $CO_2(g)$ , aqueous carbonate species, and carbonate minerals. *J. Phys. Chem. A* **2008**, *112*, 542–555.

(37) Zigan, F.; Rothbauer, R. Neutron diffraction measurements of brucite. *Neues Jahrbuch fuer Mineralogie. Monat-shefte* **1967**, *4–5*, 137–143.

(38) Busing, W. R.; Levy, H. A. Neutron diffraction study of calcium hydroxide. *J. Chem. Phys.* **1957**, *26*, 563–568.

(39) Wilson, E. B., Jr.; Decius, J. C.; Cross, P. C. *Molecular vibrations: the theory of infrared and raman vibrational spectra*; Dover Publications Inc.: New York, NY, 1980.

(40) McQuarrie, D. A. *Statistical Mechanics*; Harper and Row Publishers: New York, NY, 1973.

(41) Criss, R. E. *Principles of stable isotope distribution*; Oxford University Press: New York, NY, 1999.

(42) Clayton, R. N.; Goldsmith, J. R.; Mayeda, T. K. Oxygen isotope fractionation in quartz, albite, anorthite, and calcite. *Geochim. Cosmochim. Acta* **1989**, *53*, 725–733.

(43) O'Neil, J. R.; Adami, L. H. The oxygen isotope partition function ratio of water and the structure of liquid water. *J. Phys. Chem.* **1969**, *73*, 1553–1558.

(44) Scott, A. P.; Radom, L. Harmonic vibrational frequencies: An evaluation of hartree-fock, møller-plestet, quadratic configuration interaction, density functional theory, and semiempirical scale factors. *J. Phys. Chem.* **1996**, *100* (41), 16502–16513.

(45) Blanchard, M.; Morin, G.; Lazzeri, M.; Balan, E. First-principles study of the structural and isotopic properties of Al- and OH-bearing hematite. *Geochim. Cosmochim. Acta* **2010**, *74*, 3948–3962.

#### ■ NOTE ADDED AFTER ASAP PUBLICATION

This paper was published ASAP on May 31, 2019 with errors in Table 1. The corrected paper was reposted on June 3, 2019.